

Total pressure losses from planar particle image velocimetry data: A practical approach for accurate wake flow assessment at turbomachinery-relevant Mach & Reynolds numbers

Original article

Article history:

Submission date: 8 November 2024 Final revision date: 1 June 2025 Acceptance date: 19 August 2024 Publication date: 25 November 2025



Check for updates

*Correspondence:

MB: martin.bitter@unibw.de

Peer review:

Single blind

Copyright:

© 2025 Bitter and Kožulović © This is an open access article distributed under the Creative Commons Attribution License (CC-BY 4.0), which permits unrestricted use, distribution, and reproduction in any medium, provided the original work is properly cited and its authors credited.

Keywords:

pressure from PIV; wake pressure loss; compressible flow; cylinder in crossflow

Citation:

Bitter M., Kožulović D. (2025). Total pressure losses from planar particle image velocimetry data: A practical approach for accurate wake flow assessment at turbomachinery-relevant Mach & Reynolds numbers. Journal of the Global Power and Propulsion Society. 9: 249–261. https://doi.org/10.33737/jgpps/205784



Martin Bitter^{1,*}, Dragan Kožulović¹

¹University of the Bundeswehr Munich, Werner-Heisenberg-Weg 39, Neubiberg D-85579, Germany

Abstract

This work presents a hybrid approach for determining total pressure fields, which were reconstructed from Particle Image Velocimetry data and whose accuracy was raised through in-situ correction with probe-based reference data. The quality of this general approach is validated for turbomachinery-relevant Mach and Reynolds numbers using a cylinder in crossflow as a test case. Furthermore, the approach is applied to investigate the total pressure losses in the wake of a low-pressure turbine cascade. It is shown that the hybrid approach delivers total pressure loss fields over a wide Reynolds and Mach number range, which deviate from the highly accurate integral loss coefficients of a conventional loss traverse with probe-based measurement techniques for compressible flows by an absolute maximum of less than 2%, but which delivers results at a much higher level of spatial resolution. For incompressible flows, the deviations are almost negligible at $\leq 1\%$. The paper presents and discusses the exact methodology for both, the collection of experimental data and the outline of the developed approach.

Introduction

Characterizing the aerodynamic performance of airfoils has been based since decades on measuring the total pressure losses in the wake of the aeroshape using pressure probes, such as pitot, preston or multi-hole tubes (e.g., five-hole probe - 5HP), compare (Truckenmüller and Stetter, 1996; Börner et al., 2018). These probes are used at the location of interest, where either a single probe is traversed along a specific path or a probe rake at several locations simultaneously provides information about the distribution of the total pressure downstream of a flow body. The flow conditions in jet engines cover nearly all ranges from low-speed to supersonic Mach number conditions at Reynolds numbers from 10⁴ to 10° covering various orders of magnitude. Hence, the acquisitions of total pressure data in a wind tunnel facility covering this aerodynamic range may be delicate in terms of absolute pressure vs. sensor accuracy, settling time vs. spatial resolution or geometric parameters such as the ratio between probe head size vs. relevant test specimen dimensions (e.g., the trailing edge radius).

The pressure field is a fundamental property of fluid flow, governing important phenomena such as fluid forces, energy transfer, and flow stability. Direct measurement of pressure is often challenging, especially in

complex and dynamic flow environments. Particle Image Velocimetry (PIV) has emerged as a powerful experimental technique for quantifying fluid flow fields in various engineering applications. By capturing images of particles in seeded flows illuminated by laser light, PIV enables researchers to obtain velocity vector fields with high spatial and temporal resolution (Adrian and Westerweel, 2011; Raffel et al., 2018). While velocity information is crucial for understanding flow dynamics, the derivation of pressure fields from PIV data is equally important for comprehensive flow characterization and analysis. In recent years, the hardware development as well as the derivation of computational methods enabled the calculation of pressure fields derived from PIV based on different numerical approaches and boundary conditions, Charonko et al. (2010), van Oudheusden (2013), van Gent et al. (2017), and Tagliabue et al. (2016). Consequently, there has been considerable interest in developing techniques throughout various fields of application to infer pressure fields from velocity data obtained via PIV measurements, Ragni et al. (2009), de Kat et al. (2009), and Jacobi et al. (2022). These methods can be broadly classified into two categories: inviscid and viscous formulations. For inviscid formulations, the pressure field is obtained by solving simplified versions of the Navier-Stokes equations, neglecting viscous effects.

The application of the presented approach to viscous and even non-adiabatic flows is also part of the present research, even knowing that compromises in terms of accuracy are requisite, see e.g. van Oudheusden (2008). On the other hand, viscous formulations aim to account for the influence of viscosity on the flow field by solving additional equations or imposing constraints based on physical principles. Common approaches include the Navier-Stokes equations with appropriate boundary conditions, integral methods such as the pressure Poisson equation, and optimization-based techniques utilizing velocity and continuity constraints.

Both these well-established experimental approaches (5HP and PIV) will be merged within this paper, which aims to deliver a practical approach for the estimation of total pressure losses in wake-dominated flows such as individual airfoil or cascade exit flows. Initial work which deals in particular with cascades operating at non-adiabatic conditions but which is based on CFD data has been presented by Rusted and Lynch (2021). In this paper, a hybrid approach is used combining local but accurate total pressure measurements and reconstructed pressure fields from PIV into a plausible total pressure field. Its high spatial resolution may be advantageous in investigating wake-dominated flows. The remainder of this report is organized as follows: The testcase and the methodology for collecting the experimental data with pressure probe traverses and PIV is presented in the section *Methodology*. The hybrid approach is presented and validated in the subsequent sections. Finally, the approach is applied to a low-pressure turbine flow field in the last section.

Methodology

The aim of this paper is to provide a practical and at the same time widely general approach that enables the determination of total pressure losses of aerodynamic test specimens - both, with high spatial resolution at descent measurement accuracy. It must be clearly stated that the authors are aware that for the aim of accurately determining local and integral total pressure losses from measuring the vessels' ambient reference pressure p_{ref} according to Table 1 and total pressures p_t upstream (index "1") and downstream (index "2") of a test specimen according to Equations 1 and 2 with P/2 = 5D for the cylinder,

$$\zeta_{loc} = \frac{p_{t,1} - p_{t,2}}{p_{t,1} - p_{ref}},\tag{1}$$

$$\zeta_{int,x} = \frac{1}{P} \sum_{-P/2}^{P/2} \zeta_{loc}(x/D, y/D) \Delta(y/D),$$
 (2)

the choice and combination of measurement methods presented here is inferior to the highly accurate established methods, such as e.g., five-hole probes (5HP), as discussed in Truckenmüller and Stetter (1996), Hoenen et al. (2012), and Börner et al. (2018). However, assuming a slightly reduced accuracy is accepted, the presented approach offers enormous added value with regard to the spatial resolution of the reconstructed pressure fields in particular for the analysis of complex flow fields, such as they can occur in linear blade cascades operating at transonic conditions. Such cascade flows are usually extensively qualified in the High-Speed Cascade Wind Tunnel (HGK) at the University of the Bundeswehr in Munich. On the one hand, the presented approach is intended to expand the offered portfolio of measurement techniques and, to enable more in-depth aerodynamic analysis of complex flow processes on the other hand.

Table 1. Aerodynamic reference values at operating points and boundary conditions for pressure calculation in DaVis; the reference length for Re_D is the cylinder diameter D = 10 mm.

		Mach Number $\mathit{Ma}[-]$			
		0.3	0.5	0.7	0.85
Reynolds Number Re _D [–]	10,000	$p_{t1} = 14.7 \text{kPa}$	9.61 kPa	7.57 kPa	6.83 kPa
		$p_{ref}=13.8\mathrm{kPa}$	8.09 kPa	5.46 kPa	4.26 kPa
		$q_{ref}=0.89\mathrm{kPa}$	1.51 kPa	2.11 kPa	2.57 kPa
		$T_{t1} = 293.2 \mathrm{K}$	293.1 K	293.1 K	293.1 K
		$\rho_{ref} = 0.167 \text{kg/m}^3$	0.101 kg/m ³	0.071 kg/m ³	0.058 kg/m ³
	50,000	77.11 kPa	49.56 kPa	39.06 kPa	35.20 kPa
		72.42 kPa	41.76 kPa	28.16 kPa	21.97 kPa
		4.69 kPa	7.80 kPa	10.89 kPa	13.22 kPa
		293.2 K	293.2 K	293.1 K	293.1 K
		0.876 kg/m ³	0.521 kg/m ³	0.368 kg/m ³	0.299 kg/m ³
	80,000		82.76 kPa	65.29 kPa	58.92 kPa
			69.76 kPa	47.05 kPa	36.73 kPa
			13.00 kPa	18.24 kPa	22.16 kPa
			303.2 K	303.2 K	303.2 K
			0.842 kg/m ³	0.594 kg/m ³	0.483 kg/m ³

The HGK is a continuously operating wind tunnel, which enables experimental investigations of turbomachinery bladings under engine-relevant flow conditions (Mach and Reynolds numbers, turbulence intensity), see Niehuis and Bitter (2021). The operating map of the test facility is shown in Figure 1. The wide range of Mach and Reynolds numbers is enabled by the fact that the ambient pressure in the test facility can be varied between $p_{ref} = 4 \, \text{kPa}$ and 120 kPa. An extensive database consisting of probe-based pressure measurements and planar Particle Image Velocimetry (PIV) measurements at various operating points along the entire operating range of the HGK was captured and used to develop and validate a practical approach which combines local probe-based pressure information to pressure fields reconstructed from PIV data by means of a commercial state-of-the-art PIV evaluation software, LaVision (2021).

A cylinder in crossflow ($D=10~\rm mm$) served as a test case for the development of the method. The cylinder was mounted on a flat plate with a elliptical leading edge as to be seen on the left in Figure 2. The assembly was attached to the test section (height = width = 300 mm) of the HGK. The wake flow field was measured under different flow conditions using both, the planar PIV and total pressure probe traverses. The tests were performed at several Reynolds and Mach number combinations covering the whole range of aero engine conditions, from low-Re/low-Ma to high-Re/high-Ma flows as indicated by the white bullets in the operation map in Figure 1. Since the test section height of the HGK can be varied from 250 mm to 500 mm, the border marked with $H=300~\rm mm$ encloses the operation conditions which can be realized with the present setup dimensions. The aerodynamic conditions at the operating points can be found in Table 1, whereas the Reynolds number (indexed ReD) was calculated based on the cylinder diameter.

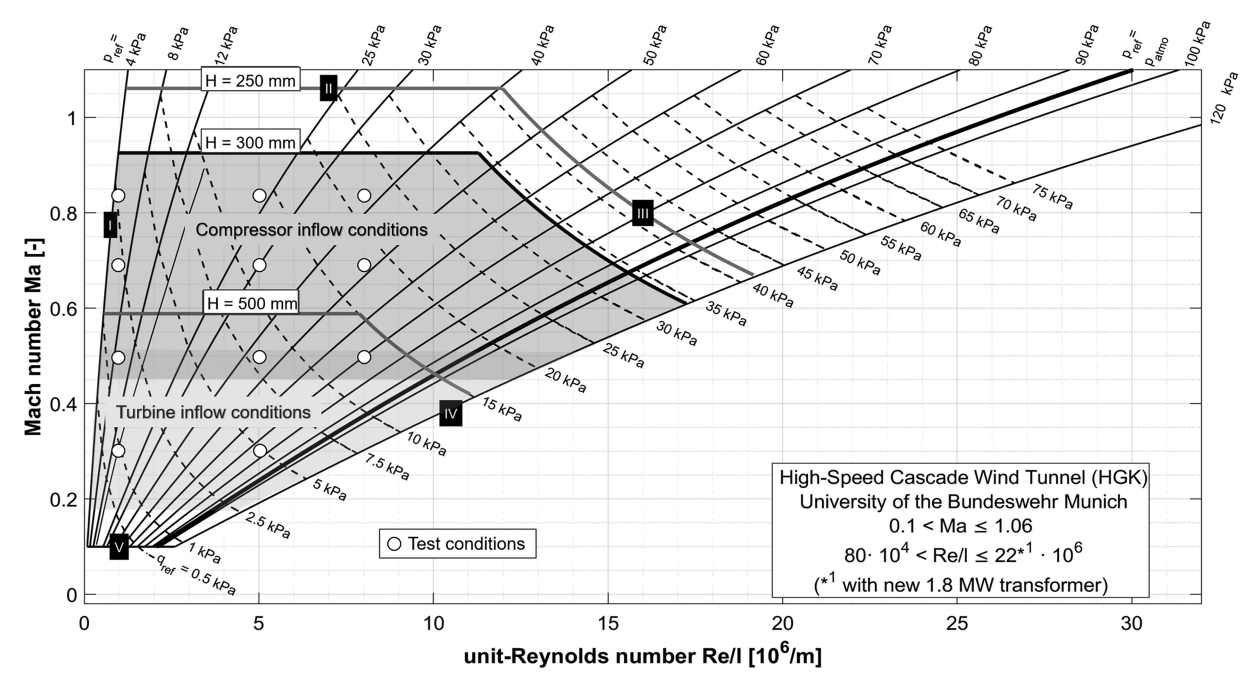


Figure 1. Aerodynamic operating conditions of the *High-speed Cascade Wind Tunnel Munich*, adapted from Niehuis and Bitter (2021). Tested operating points are labeled with $^{\circ}$. Operation limits: "I" - min. p_{ref} ; "II" - max. compressor speed; "III" - max. electrical power; "IV" - max. p_{ref} ; "V" - min. compressor speed.

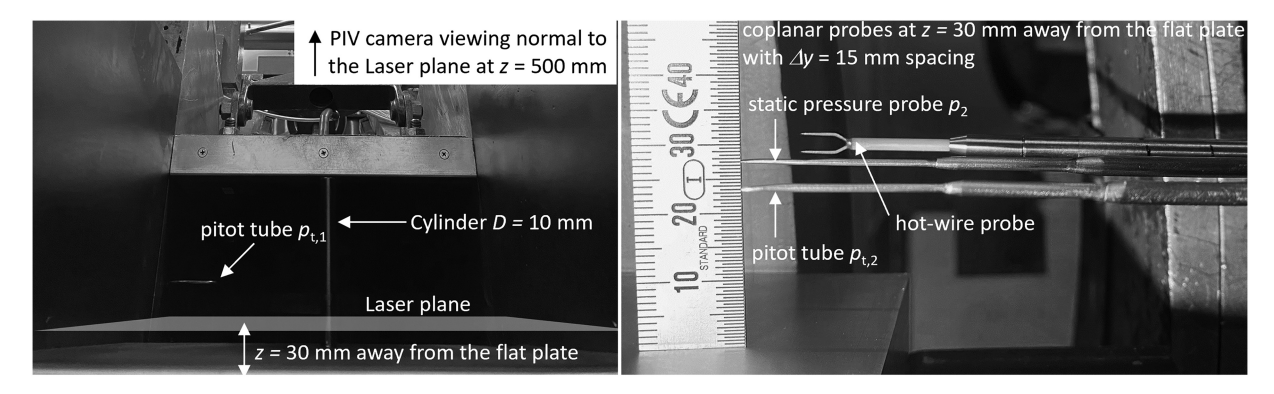


Figure 2. Left: Upstream view towards the cylinder mounted on the flat plate at the test section outlet of the HGK. The PIV Laser plane as well as the probe traverses were positioned z = 30 mm lifted away from the flat plate; Right: The probe rake comprising a total pressure, a static pressure and a hot-wire probe.

Pressure measurements

A probe rake comprising a pitot tube, a static pressure tube and a hot-wire probe for measuring turbulence spectra (discussion is not part of this paper) was traversed in the cylinder wake. The pitot pressure probes' head had an outer diameter of 1.2 mm and an inner diameter of 0.8 mm. Traversing was performed from x = 30 mm to 125 mm downstream of the cylinder and from y = -75 mm to +75 mm in the lateral expansion with a step size Δ from 3 to 15 mm (larger in the far wake). An areal probe traverse finally consisted of 450 measurement points. The irregular probe data spacing was interpolated to a regular grid which has identical resolution of the PIV grid, which is introduced in the next section.

The probe pressure data was acquired using differential pressure transducers in a rack-mount pressure scanner 98RK-1 from *Pressure Systems Inc.* offering a pressure range of ± 5 psi (or ± 34.5 kPa) and a full-scale accuracy of 0.05% (i.e. 17.3 Pa). The pressure operating conditions such as ambient pressure or total pressure of the wind tunnel were measured separately by using a *Mensor CPG* pressure scanner with increased measurement accuracy option of 0.001% (7.5 Pa or 10 Pa absolute uncertainty for ambient and total pressure, respectively). All pressure data were measured for 10 s sampled at 10 Hz.

PIV measurements

The general plausibility of applying particle-seeded flow diagnostics to turbomachinery flows and in particular in the HGK environment which partly operates at the density limits of the Stokes-flow conditions, was investigated in e.g., Ruck (1990) and Engel (2007) or Bitter et al. (2016). The particles' following behavior is widely sufficient for flows down to static pressure levels of $p_{ref} > 5$ kPa. Below 5 kPa the particle trajectories may be dominated by inertial effects, especially in the vicinity of strong accelerations and stream-line curvature. This pressure regime is touched at the operating point $Re_D = 10,000$ at $Ma_{exit} > 0.7$.

The PIV laser plane was introduced into the test section from the far wake behind the cylinder. An *Innolas Spitlight 1000* Nd:YAG double-frame laser provided 480 mJ optical power per pulse to illuminate the particles in the field. A scientific CMOS camera with double-shutter option was installed at a distance of 500 mm away from the laser plane. The camera was equipped with a 35 mm *Zeiss* macro lens to capture a field of view which even slightly extends the dimensions from the probes' field traverse. The field of view was calibrated with a planar calibration plate which was manually aligned with the flow field and the laser plane with an angular accuracy of better than 0.1 degree. The calibration scheme which is based on a second order polynomial as implemented in DaVis was applied for image reconstruction.

The flow was seeded with DEHS particles of 0.9 m RMS size using 2 PIVpart45 seeding generators from *PivTec*. In order to resolve the imaged particle displacement with a dynamic of around 15 px throughout the entire experimental range of operating points, the delay between both PIV frames was linearly adjusted from 2.2 to 6 s (lower for higher Mach numbers).

In order to ensure fully-converged Reynolds stress fields which are required for the application of the RANS equation in the pressure reconstruction scheme, 5,000 PIV images were captured and analyzed at each operating point. PIV data evaluation was performed with *LaVisions*' latest release of the commercially available state-of-the-art PIV software *Davis 10*. An iterative window-based cross-correlation approach which is standard approach for PIV evaluation was applied. The vector field of each PIV snap-shot was individually calculated based on a reducing interrogation window size (IWS) from 96 px down to 48 px at 75 %. From the authors' experience, this is a good compromise between spatial resolution and vector field calculation accuracy as a consequence of the particle density. The final PIV field had a spatial vector density of 0.46 mm/vector, which is about 8–10 times higher compared to a classical pressure probe traverse. Data post-processing and moderate spatial interpolation was applied in cases where required. Both, the data availability and vector validity were better than 99% for the cases of $Re_D > 10,000$. Especially, in the direct vicinity of the cylinder wake, these values suffered from low seeding density due to the dominance of inertial effects (in particular at Ma > 0.7).

Pressure reconstruction approach

The PIV software (LaVision, 2021) enables the reconstruction of the pressure field from both, instantaneous and time-averaged PIV velocity fields. Since this paper focusses on the presentation of a practical hybrid approach and the deeper assessment of the RANS-based reconstruction scheme can be found in e.g., Charonko et al. (2010), van Oudheusden (2013) or van Gent et al. (2017), the authors will skip the discussion at this position. Latest work by Nie et al. (2022) investigate major impact factors caused by PIV fields and propagate into the reconstructed pressure field.

It must be stated, that several restrictions between the implemented method in the software and the proposed application in the hybrid approach presented here, apply. Mainly, the algorithm expects an incompressible Newtonian fluid (e.g., water and air) where the density and dynamic viscosity of the working fluid are assumed to be constant. Secondly, the RANS equation requires the Reynolds stress fields to be fully-converged. The latter one can be encountered by providing a sufficiently high number of snapshots used for averaging as provided in this work. A discussion of losses and drawbacks of the first statement can be found in van Oudheusden (2008) where the pressure reconstruction method is applied to compressible high-speed flows.

Together with the marching scheme, the proposed boundary conditions are crucial for the accuracy of the reconstructed pressure field. Unless otherwise available, global static pressure values must be used for the Dirichlet condition. But, if available, the pressure distribution along a path or across a surface can serve as boundary condition, compare e.g. Tagliabue et al. (2016). The *Hybrid PPA: Hybrid Probe - PIV - Approach for Pressure Reconstruction* will be demonstrated and validated in the following, comprising from the following steps:

- 1. Provide total pressure information of a flow field at discrete reference points all over the field of interest,
- 2. Provide a statistically converged PIV vector flow field which also covers the reference points in the same field of interest.

- 3. Apply the following procedure for the reconstruction of the pressure field from PIV by using commercially available PIV software: 0. Select a valid PIV velocity field at a corresponding operating point; 1. Set a working fluid -> air with viscosity and reference density according to the operating point from Table 1; 2. Set the solver options to time-averaged pressure reconstruction; 3. apply a global average pressure boundary condition; 4. compute the pressure field.
- 4. Convert the static pressure field from 3) into a total pressure field by means of the isentropic conversion as given in Equations 3 and 4, whereas $p_{s,PIV}$ is the raw pressure field reconstructed from PIV,

$$Ma_{PIV} = \sqrt{\frac{V^2}{\gamma R T_{t,1} - \frac{\gamma - 1}{2} \cdot V^2}} \tag{3}$$

$$p_{t,PIV,loc} = p_{s,PIV} \cdot \left(1 + \frac{\gamma - 1}{2} M a_{PIV}^2\right)^{\frac{\gamma}{\gamma - 1}} \tag{4}$$

5. Use the reference point(s) from 1) to perform a polynomial in-situ correction of the calculated pressure field from 4) and evaluate the fit all through the PIV field.

Validation and discussion

The approach is designed to work generally if any valid PIV flow fields together with corresponding pressure data at reference positions in the field are available. The decision for a proper experimental PIV setup has than already been made following the general guidelines and common procedures as given by standard literature. The following section presents the validation and discussion of the approach as it was developed by using the cylinder data set. This section is followed by the discussion of the approach for total pressure loss estimation in the wake flow field of a linear low-pressure turbine (LPT) cascade.

Cylinder in crossflow

The results presented in this section are based on the 5 steps introduced in the previous chapter. The raw pressure fields, as they were calculated with LaVision (2021) by applying the outlined procedure from the previous section, serve as the starting point for further discussion. Beyond this initial discussion, only the fitted/corrected pressure data is discussed in the context of the paper. First, the raw reconstructed pressure data from PIV will be compared to classic probe-based total pressure measurements for Mach numbers ranging from 0.3 to 0.85. The data comparison is shown for selected operating conditions in Figure 3. The correlation between the probe-based total pressure versus the corresponding total pressure reconstructed from PIV is plotted on the left-hand side. It should be noted that the plots for Ma = 0.3, 0.5 and 0.7 have been shifted in y-direction for a better display by an individual offset of $\Delta p_t/p_{t,1} = 0.3$, 0.2 and, 0.1, respectively. Hence, all plots would collapse and end

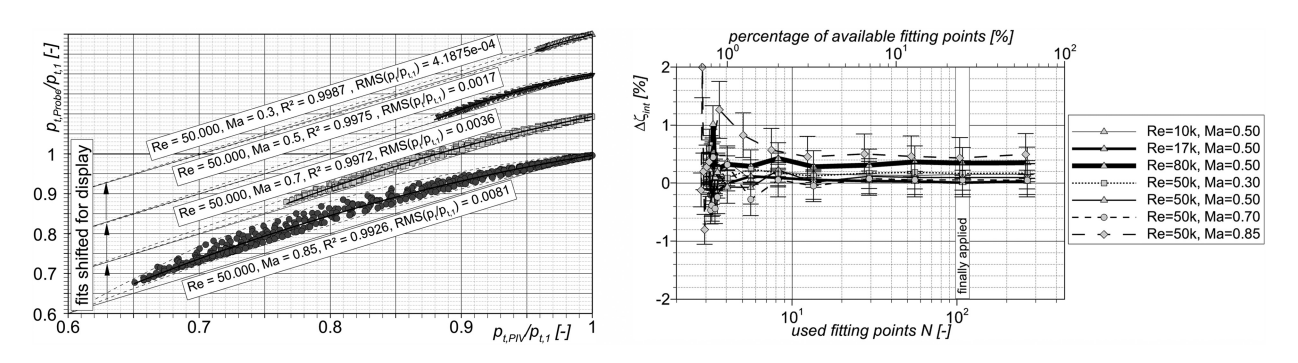


Figure 3. In-situ fits and their corresponding statistics for selected operating conditions (fit - black line, raw data - symbols). The plots on the left show the correlation between raw values reconstructed from PIV (x-axis) versus total pressures from probe measurements (y-axis) and prior to fitting. The plots on the right show the dependency of the relative deviations in pressure loss $\Delta \zeta_{int}$ between pitot probe and PIV with respect to the number of reference points which were selected to create the in-situ fits.

at $p_t/p_{t,1} = 1$. The individual symbols distinguish between the Mach numbers. When evaluating Figure 3, two key features directly stand out: on the one hand, the non-linearity of the corresponding relationships increases with increasing Mach number and, on the other hand, the fluctuation range, which is characterized by the RMS for each individual plot, also increases in the same manner. This is a major consequence of the non-consideration of compressibility effects in the pressure reconstruction scheme in LaVision (2021) which is implemented to deal with incompressible flows. In the following discussion, such a fitting function is calculated for each operation point and inversely applied to the raw total pressure data from PIV.

The dependency of the fit results in relation to the number of reference points N is plotted on the right in Figure 3. The data points were selected from the min-max pressure range in the field. This range was sub-divided into N-1 equal steps to select the corresponding pressure data, whereas the placement of the reference positions was arbitrary. As indicated by the integral difference between the fitted total pressures from PIV and the pitot probe $\Delta \zeta_{int}$ the fitting delivers stable results from already a few reference points from 10 to 20 until the fully available dataset. This means, that the number of provided reference data points is fairly low, if these probes are properly distributed to capture the full pressure range within the reconstruction field. For the generation of the polynomial fit for further discussion, a fairly large number of 100 reference data points from the pressure traverse and their corresponding counterparts from PIV have been used, and 350 points for statistical evaluation. The corresponding second-order polynomial fits and their statistics are included in the plot on the left.

Four selected planar total pressure loss fields in the wake of the cylinder are plotted in Figure 4 representing distributions from incompressible low-Re conditions (top left) to compressible high-Re in the bottom row. The top half of each sub-figure carries the probe data and compares it to the in-situ corrected pressure data from PIV on the bottom half. The local total pressure losses ζ_{loc} are calculated as introduced further above in Equation 1. In addition, the illustrations on the right-hand side contain a comparison in the form of a classical wake traverse, such as the one used to assess profile losses e.g., in a linear cascade. These traverses were extracted from both, probe and PIV plots at $\kappa/D=10$. The authors are less intended to highlight aerodynamic effects in the individual plots rather than discussing the agreement in the local and integral pressure loss coefficient. To prevent the pressure sensors from range overload, probe measurements where not carried out in the nearest vicinity of the cylinder at some operating points (esp. high Ma/high Re combinations). Since data evaluation was automated and the results were aligned among each other, all pressure field plots representing pitot data start from $\kappa/D \approx 3.5$.

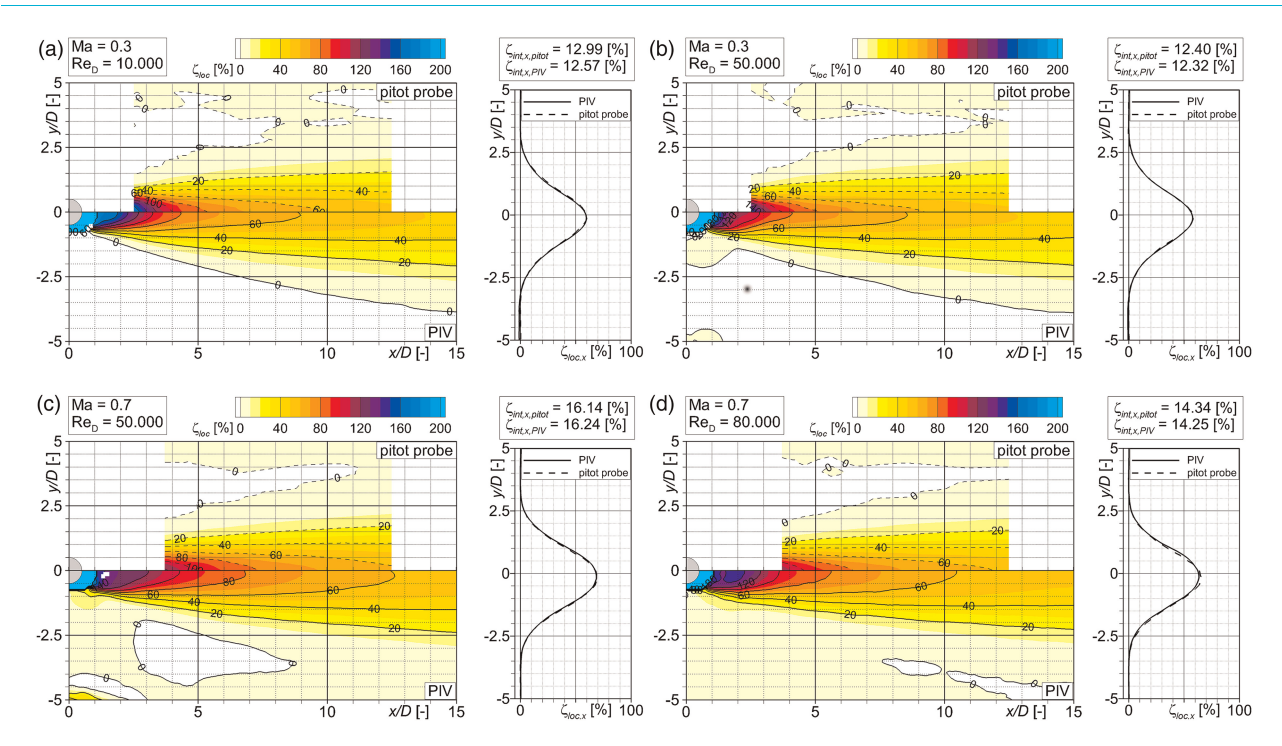


Figure 4. Comparison between total pressure losses in the wake of a cylinder measured with pitot probe in the top half of each frame (a)–(d) and reconstructed and fitted from Particle Image Velocimetry (bottom half) at different Mach and Reynolds numbers. The traverse line plots were extracted at x/D=10. (a) $Re_D=10,000$; Ma=0.3. (b) $Re_D=50,000$; Ma=0.3. (c) $Re_D=50,000$; Ma=0.3. (d) $Re_D=80,000$; Ma=0.3.

In general, a very good local and quantitative agreement can be demonstrated. It is obvious, that the wake core close to the cylinder provides larger mismatch compared to the remaining flow field. As a consequence of strong but very thin shear gradients in this area, the pressure loss production is also significantly affected by the turbulent stresses. For a highly accurate measurement of turbulent quantities, both measurement techniques are not the perfect approach, but, at least PIV (if properly applied), can help to estimate their order of magnitude. It is also known from multi-hole probe measurements, that the geometric size of the probe head and the traversing step size may have significant impact on the measured pressure data in terms of spatial resolution, especially if the flow structures become finer and the gradients get sharper, cp. Vinnemeier et al. (1990). For this reason, conventional probe traverses for total pressure loss characterization shall be performed in the mixed-out wake, were the flow is not dominated by these sharp gradients.

A criterion which may separate turbulent wakes between non mixed-out and mixed-out regions was proposed by Proudian (1964) who related the dominant turbulent fluctuations to the local wake velocity deficit according to $\Omega_z = u'^2/\Delta V^2$. In the mixed-out wake, the gradient $d\Omega_z/dx$ converges to a steady value. This does not necessarily mean, that the total pressure profile and the wake deficit is completely flattened out but rather distinguishes the axial position behind a test specimen which may not be dominated by relative turbulent fluctuations compared to the origin, e.g. directly at the trailing edge. Of course, turbulent fluctuations are present and can be higher compared to the undisturbed outer flow field. The plots in the upper rows of Figure 5 show the axial gradient of the span-wise integral of Ω along the wake length. It can be seen that the position, where the criterion converges, clearly varies between incompressible flow at Ma = 0.3 and a compressible wake at Ma = 0.7. The corresponding central and lower plots in the same figure display the axial slopes of the integral pressure loss coefficient (central plot) according to Equation 2 in comparison between PIV (solid) and probe measurements (dashed) and the relative local deviation between both experimental methods (lower plot), respectively. Again, it gets obvious that the approach performs slightly more accurate in the case of the incompressible low-speed flow. As discussed above in Figure 3, data spreading rises with increasing Mach numbers. This directly affects the inclination /offset of the in-situ fit. This may lead to a constant offset or a tilt in the reconstructed data. As also mentioned earlier, it is not the authors' claim to expect a 100 percent alignment between both data. On the other hand, an integral agreement within less than 2 percent seems valuable for the authors and their proposed approach, knowing that both measurement techniques also have their own weaknesses.

In particular transonic (wake) flows can be of interest for the application of the proposed approach since the flow field may be complex and dominated by strong velocity and pressure gradients (shocks). By means of Figure 6, the dependency of the spatial shock position on the final interrogation window size from the PIV evaluation shall be highlighted for the operation point at Ma = 0.85 and $Re_D = 50,000$. The PIV evaluation was repeated while the final IWS was changed ranging from 24 px as the finest to 96 px at the coarsest vector field, including 48 px as the standard resolution discussed throughout the entire paper. The left and right subfigures represent the axial and lateral velocity gradients for 48 px in colors, respectively. The contour line of Ma = 1 in the vicinity of the cylinder is also included. Two corresponding pressure line plots were extracted along the dashed slopes highlighted in both subfigures. These plots represent both, a cut through the shock and through the strong gradient of a transonic wakes' shear layer. In order to overcome spurious effects in the pressure reconstruction, which are linked to a bad spatial resolution of the final PIV vector field, DaVis seems to perform integration on a refined sub-grid. This approach widely eliminates the first-order dependency of the

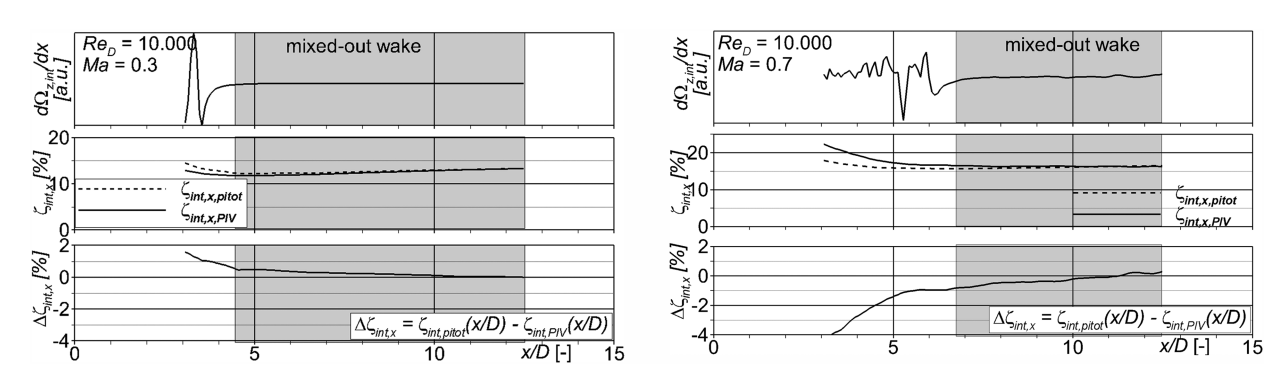


Figure 5. Spanwise-averaged wake properties showing: the axial gradient of the "mixed-out" criterion $\Omega_z = u'^2/\Delta V^2$ (top); the axial total pressure losses from PIV and pitot tube (center) and the relative difference between PIV and pitot measurements (bottom).

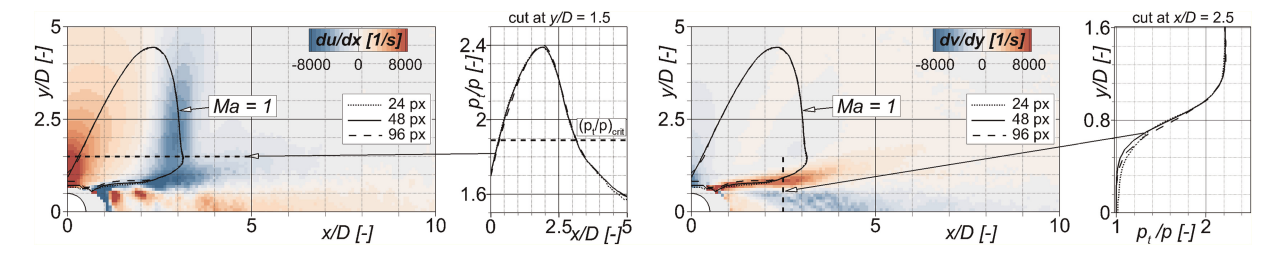


Figure 6. Shock position as a result of a PIV grid refinement study at Ma = 0.85 and $Re_D = 50,000$. The velocity gradient du/dx (left) and dv/dy (right) around the cylinder top half are plotted color-coded. Vertical and horizontal cuts through the field show reconstructed pressure ratios for PIV interrogation window sizes of 96 px, 48 px (standard for all other figures) and 24 px.

reconstructed pressure field on the final IWS. As a consequence of a reduced particle ensemble number with reduced IWS size and the corresponding raised uncertainty of the corresponding PIV vector field, the data with IWS 24 px exhibits a slightly different gradient in the wake compared to the other IWS. This effect is less pronounced in the outer flow field (cut through the shock) since the particle concentration is a-priori less in the wake compared to the outer flow. From this study it can be stated, that the proposed approach also returns reasonable results in terms of the reconstructed pressure pattern in the flow. But, as already discussed, the uncertainty of the reconstructed pressure field increases with increasing Mach number. This trend is finally highlighted by means of Figure 7. For this purpose, the integral total pressure losses of a traverse along the position x/D=10 were calculated in the same manner as above. The slopes show the corresponding pressure loss graphs for the probe measurements (filled symbols) and PIV (hollow symbols) as a primary function of the Mach number (left) and of the Reynolds number (right). The top row contains the absolute loss values. The pitot data were added up by the error bars of measurement uncertainty from the linear error propagation. The bottom row contains the mean relative deviations between the measurement techniques and the error bars were calculated from the corresponding standard deviations. (Note: By now, the PIV reconstruction tool does not provide any pressure uncertainty.)

The raising trend of the integral losses with respected to the test Mach number is evident as a consequence of rising mixing losses. The negative trend of reduced total pressure losses with increased Reynolds number is also known for viscous wake flow. As a consequence of pronounced shear forces which lead to a strong shear gradient and a reduced shear layer width, the integral losses mix out more rapidly. Both trends are well prominent in wake flows, in particular for cascades flows, whose further investigation with the proposed approach is the authors' main motivation. It is shown that both, pitot and fitted PIV pressures provide data which are in very good agreement and whose integral deviation is in the order of 1 percent or even less. The uncertainty is higher

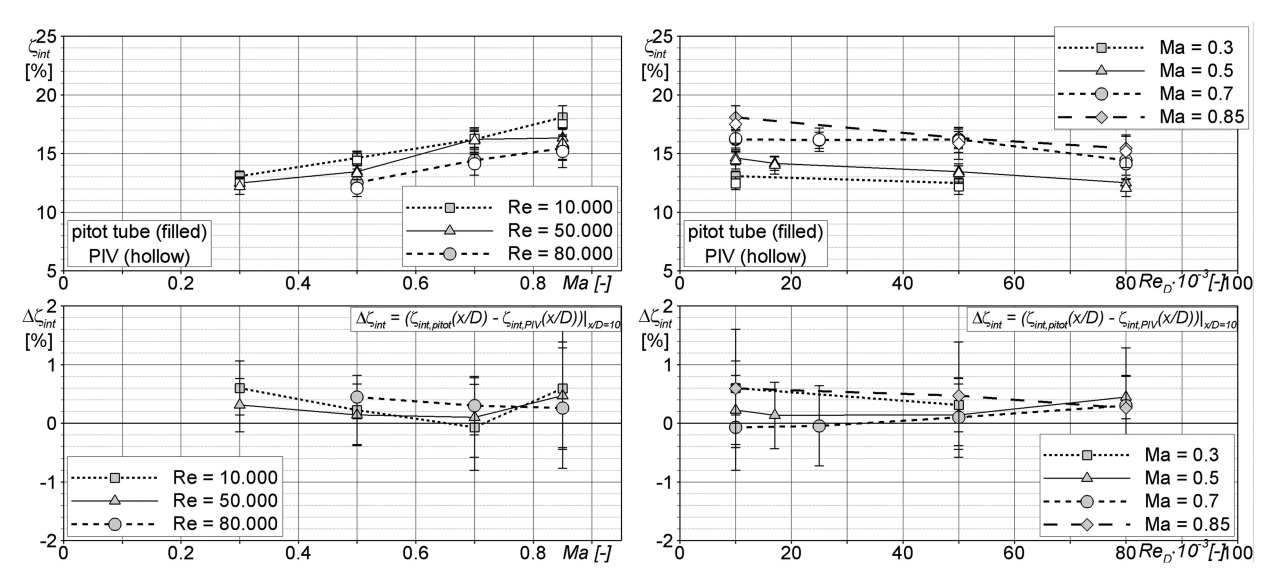


Figure 7. Comparison of integral total pressure losses between pitot probe and PIV at x/D = 10; left: Mach number effect; right: Reynolds number effect; in absolute numbers (top row) and relative deviations (bottom row).

for highest Mach numbers and at lowest ambient and dynamic pressure conditions as a consequence of a) the uncertainty of the fit raises with increased Mach number as stated above, and b) the resolution of low (dynamic) pressure differences with pressure transducers of range ± 34.5 kPa might not be the best choice but was required for the sake of keeping the test campaign in a proper time frame.

It can be stated in summary of all presented results so far, that the presented approach enables the reconstruction of reliable total pressure distributions from the PIV over a wide Reynolds and Mach number range when measured in the HGK facility. The relative deviations in the determination of the loss coefficient between the classic pressure measurement with a pressure probe (e.g., pitot or multi-hole probe) and the reconstructed distributions from PIV over the examined flow range are not larger than 2 % if the measurement uncertainty is considered, too. With respect to the simplicity of the presented approach, this high agreement is remarkably good, especially if the limitations (e.g. in the implementation of the pressure reconstruction scheme) are considered. It was also shown that the driving factor of growing uncertainty are increased compressibility effects due to the raised test Mach number, whereas the dependence on the Reynolds number appears to be comparatively small. With this knowledge, the approach appears to the authors to be valid enough to proof its performance at this level for a usage in cascade flows.

Low-pressure turbine cascade

Finally, the proposed approach is applied and cross-validated to the exit flow field downstream of a low-pressure turbine (LPT) cascade comprised of 7 blades. A detailed discussion of the cascade itself and the particular flow fields at $Ma_{exit} > 0.6$ with an inflow turbulence level of 4% is outlined in Bitter and Niehuis (2019). The wake flow field of the central blade was investigated with PIV and 5HP measurements. Pressure traverses were measured at two axial positions downstream of the cascade trailing edges, i.e. $x_{ax}/c_{ax} = [20; 80]$ %. The PIV fields' height and width extend over 1.5 blade pitches P or 1.5 axial blade lengths c_{ax} , respectively. The LPT cascade was operated at static pressures ranging from about 5 kPa at the lowest chord-based Reynolds number of 40,000 up to about 15 kPa at the highest Reynolds number of 120,000. The total pressure loss distributions in the wake at highest Reynolds number are shown on the left in Figure 8. The pressure field also embodies the local comparison of the loss traverses at 20 % and 80 % relative axial chord length x_{ax}/c_{ax} downstream the blades' trailing edge, whereas the PIV data is represented by the solid lines and the 5HP slopes by the dashed lines. The local loss values from PIV were in-situ corrected in the same manner presented above using all points from the 5HP traverses at both axial positions as in-situ fit reference data. The local values from PIV were normalized with the integral values from the 5HP measurements at position 80%. In accordance to the cylinder results from above, the agreement in the mixed-out region at 80% is remarkable. At 20%, the topology of the wake seems a bit slender for the 5HP results. This might be the consequence of the traverse position, since the wake seems not mixed out at 20% as indicated by the evaluation of the mixed-out criterion on the right in Figure 8. Anyhow, the integral losses calculated at 80% and compared between 5HP and PIV at all tested Reynolds numbers in Figure 9 agree remarkably well. The ζ values in the figure were normalized with the same reference value as above. The relative

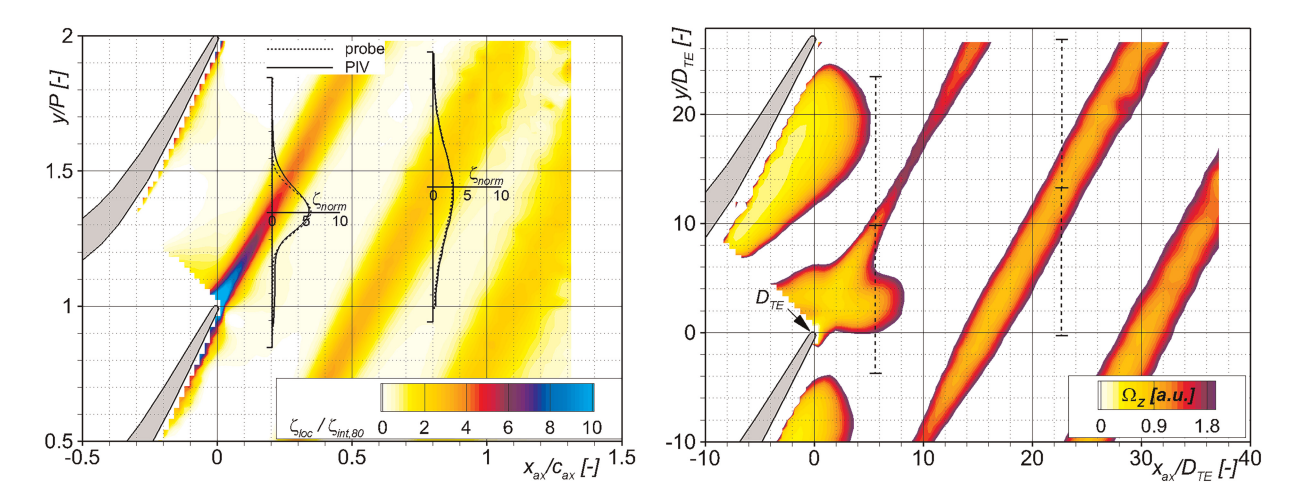


Figure 8. Left: Total pressure loss coefficient field in the wake of an LPT cascade at $Re_c = 120,000$ reconstructed from planar PIV data at $Ma_{exit} > 0.6$. The absolute values were normalized with the integral loss coefficients measured with a 5-hole probe at $x_{ax}/c_{ax} = 0.8$. Right: Color-coded evolution of the "mixed-out" criterion in direction of the LPT wake.

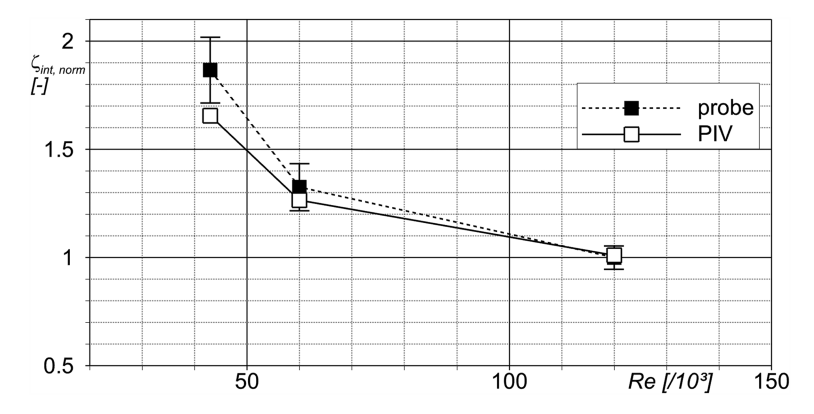


Figure 9. Comparison of integral total pressure losses in the wake of an LPT at $x_{ax}/c_{ax} = 0.8$ measured with 5HP (filled/dashed) and reconstructed from PIV (hollow/solid) at $Ma_{exit} > 0.6$.

deviations are even covered by the uncertainty of the probe measurements, except for $Re_c = 40,000$. Towards the lowest Reynolds number, the deviations grow as a consequence of the low operating density in the wind tunnel which tends to approach the limits of the stokes-flow criteria for the particle following constraint. The trend of raising pressure losses with respect to reduced Reynolds numbers not just holds for the cylinder wake flow but is also typical behavior of (LPT) airfoils in general. At all, the results presented so far proof a valid concept for total pressure loss estimation from PIV supported by local multi-hole pressure measurements.

Conclusion and outlook

The data collected as part of this work using five-hole probe measurements and PIV enabled the development of a rather simple hybrid approach that aims to determine the total pressure distributions in wake-dominated flows as precisely as possible and with high spatial resolution. The authors' main motivation is to expand the existing measurement portfolio with a compromise solution. This step shall combine the existing testing capabilities in a smart manner and expand the ability to provide information for the analysis of complex flow fields. The developed approach combines the authors' many years of know-how in optical and probe-based exploration of wake flows with state-of-the-art calculation methodology for reconstructing pressure distributions from velocity field measurements as measured with PIV.

It was shown that the presented approach delivers valid results over a wide operating range, as covered by the High-Speed Cascade Wind tunnel operated at the University of the Bundeswehr in Munich for investigations of turbomachinery bladings. The investigated flow range covered a Mach number range from 0.3 to 0.85 at 3 different Reynolds numbers. The total pressure loss coefficient reconstructed from PIV, which was in-situ-corrected by means of reference points from probe-based pressure measurements, had a maximum uncertainty of approx. 2% in the entire examined operating range. In the low-speed range at $Ma \le 0.3$, the relative deviation between both measurement techniques seems to be negligible at well below 1%.

The approach presented here is based on a simple second-order polynomial fit between known reference values and the raw pressure values reconstructed from the PIV, whereby the reconstruction scheme is actually implemented for incompressible flows. In addition, the presented approach also contains isentropic assumptions when calculating the Mach number distribution from the velocity distributions of the PIV and the conversion from static pressure to total pressure. Given the combination of all these simplifications and assumptions, the relatively high level of agreement between the results is remarkably good. The users should be aware of some key factors in the flow field, which can be summarized as:

- 1. The application of the procedure seems less accurate if the measured and/or reconstructed pressure values are part of a non-mixed-out wake flow. Here, both, the pressure probe and the PIV have their own deficit and increase the accuracy of the algorithm.
- 2. The reference probes for fitting are less dependent on their actual positions but rather that they are distributed to cover values across the entire pressure range and flow field to be reconstructed. Knowing this, a fairly low number of reference probes around 20 can deliver sufficient results.
- 3. It was shown, that the application of the approach for high-speed/transonic flows is generally possible. Nevertheless, the nature of the incompressible pressure reconstruction scheme implemented in DaVis inherently limits the validity and necessitates the careful usage and questioning of the results.

Further analyzes should show how an increase in accuracy can still be achieved. Surely, it might be expensive, not just in terms of monetary invest but also in terms of time for lessons-learned, to take this approach as a substitution for probe measurements. But a supplementary usage as a complementary testing tool to enlarge the potential information gathered from a flow field is emphasized. In particular, in regions where the probes' presence encounters the measurement accuracy, e.g. in the vicinity of walls or in the presence of sharp gradients in complex flow fields, this approach can deliver reasonably accurate results.

Nomenclature

Latin symbols

characteristic length
cylinder diameter
test section height
Ma
Mach number

N Number of data points p_s ; p_t static; total pressure P cascade pitch q dynamic pressure

R ideal gas constant = 287.15 J/(kgK)

 Re_c ; Re_D Reynolds number based on chord length or cylinder diameter D=10 mm

 T_t total temperature

V velocity vector V = [u; v] or [u; v; w] x; y axial and lateral wind tunnel coordinates

Greek symbols

γ specific heat ratio

 Δ integration step size or difference between two quantities

 $\zeta_{loc}; \zeta_{int}$ local or integral total pressure loss coefficient

 ρ fluid density

 Ω mixed-out criteria = $u'^2/\Delta V^2$

Abbreviations

5HP five-hole probe

ax axial dimension in blade coordinates

HGK High-speed Cascade Wind Tunnel at the University of the Bundeswehr in Munich

IWS Interrogation window size

exit exit condition

LPT Low-Pressure Turbine norm normalized value

PIV Particle Image Velocimetry

ref reference condition RMS root-mean-square value

Competing interests

Martin Bitter declares that he has no conflict of interest. Draga Kozulovic declares that he has no conflict of interest.

References

Adrian R. and Westerweel J. (2011). Particle Image Velocimetry. Cambridge Aerospace Series. Cambridge, UK: Cambridge University Press.

Bitter M. and Niehuis R. (2019). Effects of periodic inflow turbulence on the statistics in the wake of a linear LPT cascade at jet-engine relevant test conditions. In: 13th International Symposium on Particle Image Velocimetry – ISPIV 2019, Munich, Germany, July 22–24.

- Bitter M., Kurz J., Kähler C. J., and Niehuis R. (2016). Investigations of a low pressure turbine blade by means of simultaneous optical velocity and pressure measurements. In: 18th International Symposium on Applications of Laser Techniques to Fluid Mechanics, July 4–7, Lisbon, Portugal.
- Börner M., Bitter M., and Niehuis R. (2018). On the challenge of five-hole-probe measurements at high subsonic mach numbers in the wake of transonic turbine cascades. *Journal of the Global Power and Propulsion Society*. 2: 453–464.
- Charonko J. J., King C. V., Smith B. L., and Vlachos P. P. (2010). Assessment of pressure field calculations from particle image velocimetry measurements. *Measurement Science and Technology*. 21 (10): 105401. https://doi.org/10.1088/0957-0233/21/10/105401.
- de Kat R., van Oudheusden B., and Scarano F. (2009). Instantaneous pressure field determination around a square-section cylinder using time-resolved stereo-PIV. In: 39th AIAA Fluid Dynamics Conference, June 22–25, San Antonio, Texas, USA.
- Engel C. (2007). Untersuchung der Laufradströmung in einem Radialventilator mittels Particle Image Velocimetry (PIV). PhD thesis, Fakultät Ingenieurwissenschaften der Universität Duisburg-Essen.
- Hoenen H. T., Kunte R., Waniczek P., and Jeschke P. (2012). Measuring failures and correction methods for pneumatic multi-hole probes, ASME turbo expo: power for land, sea, and air.
- Jacobi G., Thill C., and Huijsmans R. (2022). Pressure reconstruction from PIV measurements in the bow region of a fast ship. *Ocean Engineering*. 252: 110318. https://doi.org/10.1016/j.oceaneng.2021.110318.
- LaVision (2021). Pressure from PIV (Poduct Manual for DaVis 10.2). Göttingen, Germany: LaVision GmbH.
- Nie M., Whitehead J. P., Richards G., Smith B. L., and Pan Z. (2022). Error propagation dynamics of PIV-based pressure field calculation (3): what is the minimum resolvable pressure in a reconstructed field? *Experiments in Fluids*. 63 (11): 168. https://doi.org/10.1007/s00348-022-03512-8.
- Niehuis R. and Bitter M. (2021). The high-speed cascade wind tunnel at the Bundeswehr University Munich after a major revision and upgrade. *International Journal of Turbomachinery, Propulsion and Power.* 6 (4): 41. https://doi.org/10.3390/ijtpp6040041.
- Proudian A. P. (1964). Mixing and fluctuations on a turbulent wake. Technical report, Heliodyne Corporation Los Angeles, CA.
- Raffel M., Willert C. E., Scarano F., Kähler C. J., Wereley S. T. et al. (2018). Particle Image Velocimetry: A practical guide. 3rd ed. Switzerland: Springer Verlag Cham.
- Ragni D., Ashok A., van Oudheusden B. W., and Scarano F. (2009). Surface pressure and aerodynamic loads determination of a transonic airfoil based on particle image velocimetry. *Measurement Science and Technology.* 20 (7): 074005. https://doi.org/10.1088/0957-0233/20/7/074005.
- Ruck B. (1990). Influence of tracer particle size on flow information in laser Doppler anemometry (in German). *tm Technisches Messen*. 57: 284–295. https://doi.org/10.1524/teme.1990.57.jg.284.
- Rusted A. and Lynch S. (2021). Determining total pressure fields from velocimetry measurements in a transonic turbine Flowfield. In: Vol. Volume 2B: Turbomachinery Axial Flow Turbine Aerodynamics; Deposition, Erosion, Fouling, and Icing of ASME Turbo Expo: Power for Land, Sea, and Air. p. V02BT32A009.
- Tagliabue A., Bitter M., Scharnowski S., and Kähler C. J. (2016). Surface pressure determination: a comparison between PIV-based methods and PSP measurements. In: 18th International Symposium on Applications of Laser Techniques to Fluid Mechanics, July 4–7, Lisbon, Portugal.
- Truckenmüller F. and Stetter H. (1996). Measurement errors with pneumatic probes behind guide vanes in transonic flow-fields, MTT1396-A307. In: 13th Symposium on Measuring Techniques for Transonic and Supersonic Flow in Cascades and Turbomachines, September, 5–6, Zurich, Switzerland.
- van Gent P. L., Michaelis D., van Oudheusden B. W., Weiss P. E., de Kat R. et al. (2017). Comparative assessment of pressure field reconstructions from particle image velocimetry measurements and lagrangian particle tracking. *Experiments in Fluids*. 58 (4): 032001. https://doi.org/10.1007/s00348-017-2324-z.
- van Oudheusden B. W. (2008). Principles and application of velocimetry-based planar pressure imaging in compressible flows with shocks. *Experiments in Fluids*. 45 (4): 657–674. https://doi.org/10.1007/s00348-008-0546-9.
- van Oudheusden B. W. (2013). PIV-based pressure measurement. *Measurement Science and Technology*. 24 (3): 032001. https://doi.org/10.1088/0957-0233/24/3/032001.
- Vinnemeier F., Simon L., and Koschel W. (1990). Correction method for the head geometry influence of a five-hole pressure probe on the measurement results (in German). tm Technisches Messen. 57: 296–303. https://doi.org/10.1524/teme.1990.57.jg.296.